Physics and Chemistry of the Earth 98 (2017) 49–61

Contents lists available at ScienceDirect

Physics and Chemistry of the Earth

journal homepage: www.elsevier.com/locate/pce

S-wave velocity measurement and the effect of basin geometry on site response, east San Francisco Bay area, California, USA

Koichi Hayashi [a,*], Mitchell Craig [b]

[a] Geometrics, 2190 Fortune Drive, San Jose, CA 95131, USA
[b] Department of Earth and Environmental Sciences, California State University, East Bay, 25800 Carlos Bee Blvd., Hayward, CA 94542, USA

A R T I C L E I N F O

Article history:
Received 12 February 2016
Received in revised form
19 May 2016
Accepted 11 July 2016
Available online 22 July 2016

Keywords:
S-wave velocity
Site effects
Surface wave method
Ambient noise
Finite-difference method
San Francisco Bay area

A B S T R A C T

We measured S-wave velocity profiles at eleven sites in the east San Francisco Bay area using surface wave methods. Data acquisition included multichannel analysis of surface waves using an active source (MASW), a passive surface-wave method using a linear array of geophones (Linear-MAM), and a two-station spatial autocorrelation method (2ST-SPAC) using long-period accelerometers. Maximum distance between stations ranged from several hundred meters to several kilometers, depending on the site. Minimum frequency ranged from 0.2 to 2 Hz, depending on the site, corresponding to maximum wavelengths of 10 to 1 km. Phase velocities obtained from three methods were combined into a single dispersion curve for each site. A nonlinear inversion was used to estimate S-wave velocity profiles to a depth of 200–2000 m, depending on the site. Resultant S-wave velocity profiles show significant differences among the sites. On the west side of the Hayward fault and the east side of the Calaveras fault, there is a low velocity layer at the surface, with S-wave velocity less than 700 m/s, to a depth of approximately 100 m. A thick intermediate velocity layer with S-wave velocity ranging from 700 to 1500 m/s lies beneath the low velocity layer. Bedrock with S-wave velocity greater than 1500 m/s was measured at depths greater than approximately 1700 m. Between the Hayward Fault and the Calaveras Fault, thicknesses of the low velocity layer and the intermediate velocity layer are less than 50 m and 200 m respectively, and depth to bedrock is less than 250 m. To evaluate the effect of a lateral change in bedrock depth on surface ground motion due to an earthquake, a representative S-wave velocity cross section perpendicular to the Hayward fault was constructed and theoretical amplification was calculated using a viscoelastic finite-difference method. Calculation results show that the low frequency (0.5–5 Hz) component of ground motion is locally amplified on the west side of the Hayward fault because of the effect of two-dimensional structure.

1. Introduction

1.1. Applications of surface wave methods

Surface ground motion from earthquakes is highly dependent on subsurface geological structure. The local site effect may be defined as the effect of subsurface geological structure on surface ground motion. To estimate the local site effect, S-wave velocity to a depth of several tens of meters, such as the average S-wave velocity down to 30 m (V_S30), is very popular worldwide. Observations from several recent severe earthquakes and subsequent research (e.g. Kawase, 1996; Hayashi et al., 2008), however, have revealed that two- or three-dimensional deep S-wave velocity structure (to a depth of several km) has a large effect on intermediate to long period (0.5–5 s) ground motion in tectonic basins, such as the San Francisco Bay area. Most studies on basin velocity structure rely on geological information, surface and borehole geophysical data and observed earthquake records. In general, geophysical data and seismic stations are too sparsely distributed and much of the borehole data is too shallow to adequately characterize deep S-wave velocity structure. To establish more accurate basin velocity structure, there is a need for more closely spaced deep S-wave velocity measurements.

1.2. Development of analysis methods

The use of surface waves for near-surface S-wave velocity

* Corresponding author.
E-mail addresses: khayashi@geometrics.com (K. Hayashi), mitchell.craig@csueastbay.edu (M. Craig).

http://dx.doi.org/10.1016/j.pce.2016.07.001
1474-7065/

estimation has undergone significant development during the past decade (e.g., Tokimatsu, 1997). Spectral analysis of surface waves (SASW) has been used to determine one-dimensional (1D) S-wave velocity profiles to a depth of 100 m (Nazarian et al., 1983). SASW surveys employ a shaker or a vibrator as sources, and calculate phase differences between two receivers via cross correlation. Park et al. (1999a, 1999b) proposed a multichannel analysis of surface waves (MASW) method, which determines phase velocities directly from multichannel surface wave data after transforming waveform data from the time-distance domain into the phase velocity–frequency domain. MASW is much better than SASW for recognition of dispersion curves and distinguishing the fundamental mode of Rayleigh wave from other modes, such as higher modes and body waves. In addition, MASW can avoid spatial aliasing, which is a problem in SASW. Xia et al. (1999a) and Miller et al. (1999) applied MASW to shot gathers along a survey line and delineated pseudo two-dimensional (2D) S-wave velocity sections.

1.3. Ambient noise methods

During the past few decades, considerable progress has been made towards the development of seismic methods utilizing ambient noise. Because the ambient noise is generated by sources on the ground surface, the ambient noise mainly consists of surface waves, and the vertical component of the ambient noise can be considered as Rayleigh waves. Therefore, it is reasonable that the dispersion curve of the vertical component of the ambient noise is the dispersion curve of Rayleigh waves. Aki (1957) investigated ambient noise as surface waves and proposed a theory of spatial autocorrelation (SPAC). A passive surface wave method, or microtremor array measurements (MAM) based on SPAC was developed by Okada (2003) in order to estimate deep S-wave velocity structure. Ambient noise is also utilized in seismic interferometry (Wapenaar, 2004). The passive surface wave method or microtremor array measurements (Okada, 2003; Asten, 2006; Ikeda et al., 2012), in which ambient noise is used as surface waves, is particularly effective for estimation of deep S-wave velocity structure because the method does not require an artificial source and the depth of investigation can easily be extended by increasing the size of the array. Large aperture MAM surveys have been widely used during the past 15 years particularly in Japan for estimating S-wave velocity structure to a depth of several km. Such investigations revealed that an abrupt change of the depth of basement caused a concentration of damage in the Kobe, Japan earthquake of 1995 (Tokimatsu et al., 1996).

1.4. Array patterns

For SPAC analysis, the ideal array pattern should be isotropic and include a range of offsets spanning the range of wavelengths of interest. An isotropic array pattern is one that provides the same response regardless of the direction of the incoming wavefield. A simple circular array has an isotropic response but does not contain an even distribution of offsets, thus its wavenumber response has fairly large sidelobes beyond the first minimum. Arrays of concentric circles or nested triangles have smaller sidelobes (Mykkeltveit et al., 1983; Vermeer, 2002) and are ideal for SPAC surveying. Garofalo et al. (2016a) used a variety of different areal arrays for the acquisition of passive surface wave data, including concentric circles, nested triangles, and L-shaped arrays. The use of an isotropic array ensures that velocities will be accurately estimated, even in the case of anisotropic noise, i.e. noise arriving from a limited range of directions.

However, the differences between isotropic and anisotropic arrays do not have a significant impact on data quality in some situations (e.g. Yokoi et al., 2006; Hayashi, 2009; Craig and Genter, 2006). For example, an L-shaped array provides phase velocities with sufficient accuracy for some applications and offers a practical alternative to an isotropic array for SPAC analysis at the sites where an isotropic array cannot be deployed. Margaryan et al. (2009) applied SPAC to data recorded using a linear array with two sensors (2ST-SPAC) and compared the performance of the linear array in comparison with a triangular array. Louie (2001) presented the ReMi method, a passive method in which ambient noise surface waves is recorded using a linear array. Waveform data are transformed to the frequency domain using a tau-p transform, and the fundamental mode dispersion curve is picked along the ridge of maximum slowness (minimum apparent velocity). Stephenson et al. (2005) compared shear-wave velocities obtained using ReMi and MASW with those measured by suspension logging. Garofalo et al. (2016b) compared velocity profiles measured using several surface wave methods, including both active and passive methods, with velocities measured using borehole methods.

Passive methods in general and those using anisotropic or linear arrays in particular, are most effective in urban environments that have a sufficient level of ambient noise with a reasonable degree of isotropy. In practice, perfectly isotropic arrays are difficult to implement for many routine field investigations because they require access over an extensive area. L-shaped or linear arrays offer a practical alternative as they can easily be laid out along public roadways.

1.5. Motivation of study

We measured S-wave velocity profiles at eleven sites in the east San Francisco Bay area using active and passive surface wave methods. The 2ST-SPAC and linear array were used to carry out passive measurements in urban areas. The sites were placed around the Hayward fault and the Calaveras fault. The 30-year probabilities of magnitude 6.7 or greater earthquakes on the Hayward-Rodgers Creek and Calaveras faults have been estimated at 32% and 25%, respectively (Field et al., 2015). These faults run through densely populated areas and knowledge of a detailed two- or three-dimensional S-wave velocity structure along the faults is needed in order to estimate local site effects due to a potential earthquake. This paper summarizes data obtained by the surface wave methods, shows S-wave velocity profiles calculated by inversion, and discusses the effect of 2D S-wave velocity structure on surface ground motion.

2. Data acquisition

2.1. Sites of investigation

The sites of investigation are shown in Fig. 1. The Hayward and Calaveras faults are oriented northwest-southeast. Displacement along the faults is primarily strike slip. The two faults bound the East Bay Hills block, which has 50–500 m of topographic relief. As shown on the site map (Fig. 1), seven sites are located on the west side of the Hayward fault (11, 57, 65, 66, 67, 68 and 84), two sites are located on the east side of the Calaveras fault (59 and 69), and two sites are located between the two faults (58 and 64).

2.2. Data acquisition

Data acquisition methods included multichannel analysis of surface waves using an active source (MASW), a passive surface wave method using geophones in a linear array (Linear-MAM), a two-station spatial autocorrelation method (2ST-SPAC), and the horizontal to vertical spectral ratio (HVSR) method. The 2ST-SPAC

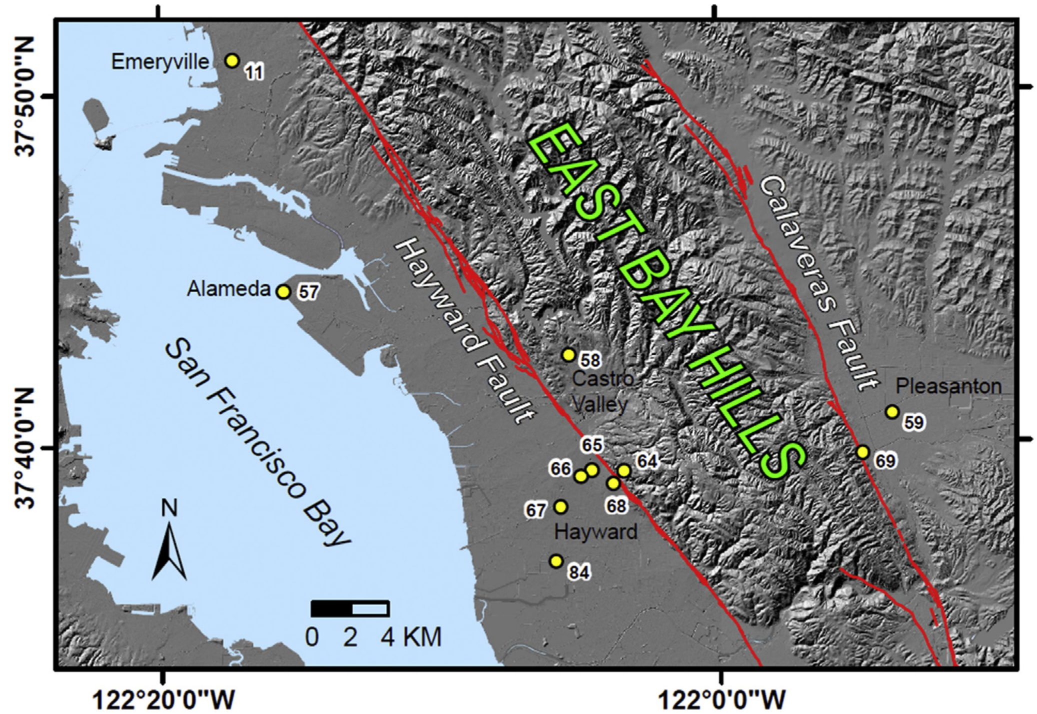

Fig. 1. Sites of investigation. 11 – Emeryville, 57 – Alameda, 58 – Castro Valley, 59 – Pleasanton, 64 – CSU East Bay, 65 – Charles Ave, 66 – Huntwood Ave, 67 – Southgate Park, 68. Cemetary, 69 – Alviso Adobe, 84 – Eden Shores Park.

and HVSR data were acquired using long-period accelerometers, described in greater detail below.

2.3. Multichannel analysis of surface waves (MASW)

MASW surveys (Park et al., 1999a; Xia et al., 1999a) were conducted using 24 or 48 receivers, 4.5 Hz vertical geophones, and a 1 or 2 m receiver interval. A 10 kg sledgehammer was used as an energy source. Several shots were stacked to increase signal to noise ratio. Shot records with a sample rate of 1 ms and data length of 2.0 s were recorded using a Geometrics Geode seismographic system. Minimum frequency obtained from the method is 5–20 Hz, depending on the site.

2.4. Passive surface-wave method using geophones in a linear array (Linear-MAM)

Ambient noise was also recorded with the geophone array used for the MASW survey described above. About 10 min of ambient noise data with a 2 ms sampling rate were recorded at each site. Minimum frequency obtained from the method is approximately 2–5 Hz, depending on the site.

2.5. Two-station spatial autocorrelation (2ST-SPAC)

Several recent studies showed that S-wave velocity profiles can be determined to a depths of 2000–3000 m by using two sensors and the spatial autocorrelation (SPAC) method in the southern portion of the San Francisco Bay area (Hayashi and Underwood, 2012a, 2012b), the Los Angeles Basin, California (Hayashi et al., 2013b), and Seattle and Olympia, Washington (Hayashi et al., 2013a). We used the same method using two or three sensors in the present study to obtain lower frequency phase velocities.

At each site, one seismograph was established at a fixed location with microtremor data acquired for the duration of the survey. Microtremor data were also acquired with one or two additional seismographs at several different locations with a range of separations from the fixed instrument. Maximum separation ranged from 200 to 2300 m, depending on the site. At each measurement location, we recorded microtremor data for an interval ranging from 10 min to 1 h using a 10 ms sample rate, for a total of several hours of data acquisition per site. As the separation of seismographs increased, the record length of ambient noise was increased. An example array from Site 57 (Alameda) is shown in Fig. 2. Data acquisition was performed during the daytime. Seismographs were placed in relatively quiet locations such as parks and residential areas. OYO McSEIS-MT Neo seismographs (Resolution: 1 μG, Sensitivity: 2.0 V/G, Range: +/−4G) were used for data acquisition. The seismographs utilize three-component accelerometers and include a GPS clock to synchronize data between multiple seismographs. Recorded three-component ambient noise data was used for the horizontal to vertical spectral ratio (HVSR) analysis.

3. Data processing

3.1. Phase velocity calculation

A phase shift and stack procedure was used to calculate dispersion curves from shot gathers obtained by MASW (Park et al., 1999a) and spatial autocorrelation (SPAC) was used to calculate dispersion curves from ambient noise obtained by Linear-MAM and 2ST-SPAC.

The vertical component of ambient noise was used for SPAC. Recorded ambient noise data were divided into several time blocks with overlaps. Each block consists of a data length of 81.92 s. Several blocks containing nonstationary noise were rejected before processing. Complex coherence was first calculated for each block, then the real part of the coherence for all blocks was averaged to obtain the spatial autocorrelation (SPAC) (Hayashi et al., 2013b).

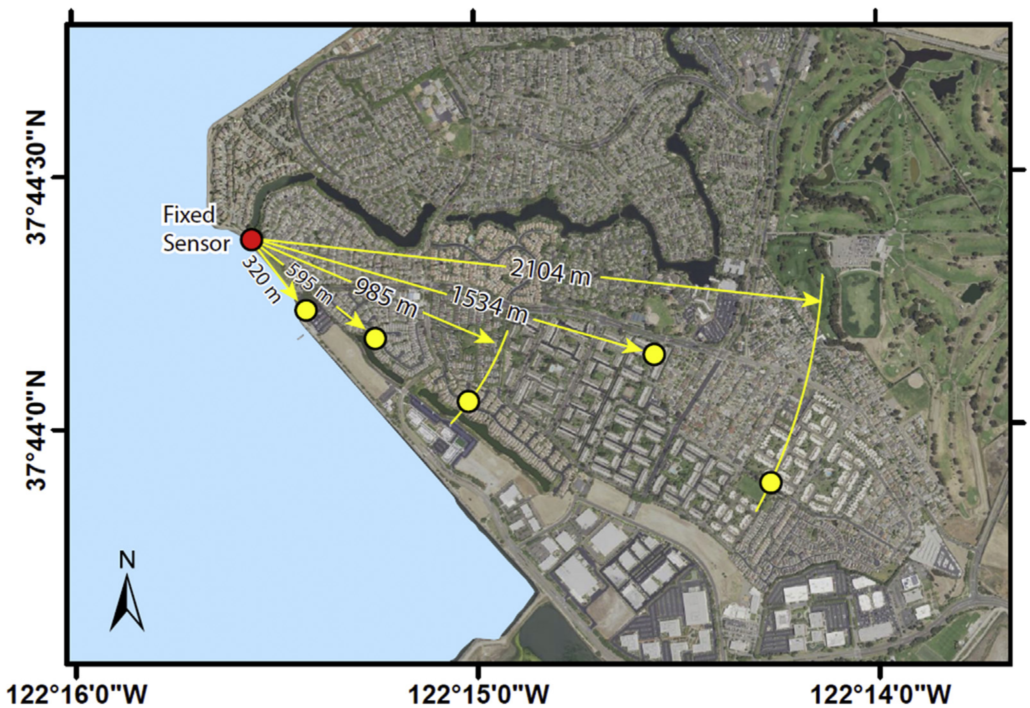

Fig. 2. Example of 2ST-SPAC array configuration at Site 57 (Alameda). One sensor (red circle) is fixed and a second (yellow) is placed at a series of locations with progressively greater separation distances: 320 m, 595 m, 1534 m, and 2104 m. Ambient noise is recorded continuously by the first sensor and for a limited period of time at each location by the second sensor. (For interpretation of the references to colour in this figure legend, the reader is referred to the web version of this article.)

The velocity which minimizes the error between the observed SPAC and a Bessel function of the first kind (zero order) was considered to be the phase velocity (Aki, 1957).

Dispersion curves obtained by the three different methods are in excellent agreement in the frequency ranges where they overlap (Fig. 3). The good agreement in the region of overlap between the MASW (active) and Linear-MAM (passive) datasets provides a confirmation that the linear array is detecting sufficient ambient noise in the inline direction to measure the true velocity. If the ambient noise field were anisotropic, arriving at an angle not parallel to the array, apparent velocity would exceed true velocity. Maximum wavelengths obtained using the 2ST-SPAC, Linear-MAM and MASW were about 10,000, 150 and 30 m, respectively. As a rule of thumb, the penetration depth of the surface wave method is about one-half to one-third of the maximum Rayleigh wave wavelength (e.g. Xia et al., 1999b). The penetration depth of the 2ST-SPAC method is much greater than that of conventional surface wave methods, such as MASW or ReMi. Phase velocities obtained from three methods were combined to produce a single dispersion curve for each site.

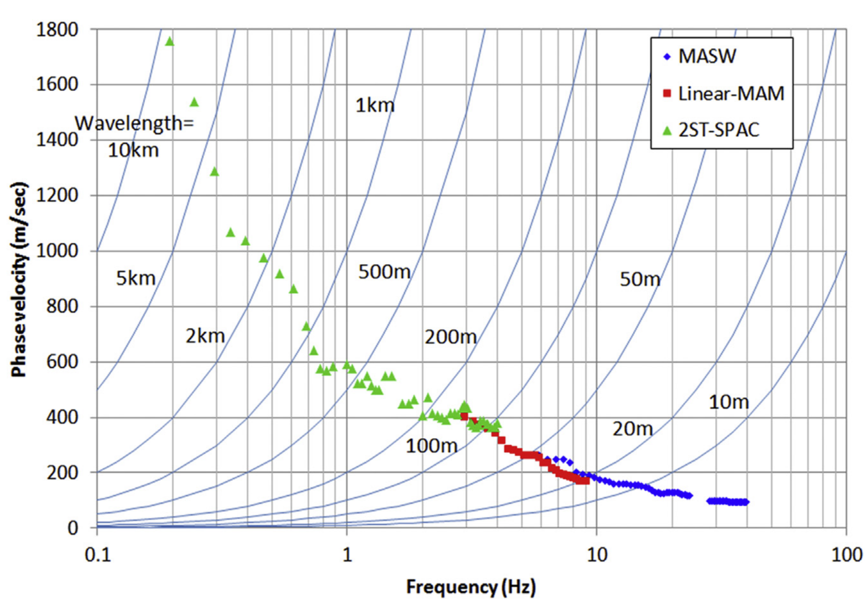

Fig. 3. Comparison of dispersion curves at Site 59 (Pleasanton).

3.2. Inversion

An inversion scheme (Suzuki and Yamanaka, 2010) was applied to the observed dispersion curves to develop S-wave velocity profiles for the eleven sites. During the inversion, the observed data were the phase velocities of a dispersion curve, the horizontal to vertical spectral ratio (HVSR), and the peak frequency of the HVSR. The unknown parameters were layer thickness and S-wave velocity. A genetic algorithm (Yamanaka and Ishida, 1995) was used for optimization. The search area for the inversion was determined based on initial velocity models created by a simple wavelength transformation in which wavelengths calculated from phase velocity and frequency pairs were divided by three and mapped as depth.

The theoretical phase velocity and HVSR were defined as an effective mode that was generated by calculating the weighted average of the fundamental mode and higher modes (up to the 5th mode) based on the medium response. The effective mode of theoretical phase velocity can be calculated by the following procedure (Obuchi et al., 2004; Ikeda et al., 2012). First, the root mean square error (RMSE) between the Bessel function and the theoretical SPAC coefficients is calculated by the following equation by changing the phase velocity $c(\omega)$

$$RMSE(c,\omega) = \sqrt{\left[J_0\left(\frac{\omega}{c(\omega)}r\right) - \sum_{i=0}^{n}\frac{P_i(\omega)}{P(\omega)}J_0\left(\frac{\omega}{c_i(\omega)}r\right)\right]^2} \tag{1}$$

$$\frac{P_i(\omega)}{P(\omega)} = \frac{c_i(\omega)A_i^2(\omega)}{\sum_{i=0}^{n}c_i(\omega)A_i^2(\omega)} \tag{2}$$

where ω is angular frequency, r is separation of sensors, n is the number of modes, and J_0 is the Bessel function of the first kind of zero order, P_i, A_i and c_i are power, medium response and phase velocity of ith mode respectively. The c_i and A_i can be calculated from a 1D velocity profile. Next, the velocity that minimizes RMSE in equation (1) can be considered to be the theoretical effective mode of phase velocity $c_e(\omega)$ at angular frequency ω. These effective modes correspond to the observed phase velocity even if higher modes of surface waves are predominant.

The effective mode of theoretical HVSR of surface waves $H/V_{Se}(\omega)$ can be calculated by following equations presented by Arai and Tokimatsu (2000).

$$H/V_{Se}(\omega) = \sqrt{\frac{P_{HS}(\omega)}{P_{VS}(\omega)}} \tag{3}$$

$$P_{HS}(\omega) = P_{HR}(\omega) + P_{HL}(\omega), \tag{4}$$

$$P_{HR}(\omega) = \sum_{i=1}^{n}\left(\frac{c_{R_i}(\omega)A_{R_i}(\omega)}{\omega}\right)^2\left(\frac{u}{w}\right)_i^2(\omega)\left\{1+\left(\frac{\alpha^2}{2}\right)\left(\frac{u}{w}\right)_i^2(\omega)\right\} \tag{5}$$

$$P_{VS}(\omega) = P_{VR}(\omega) = \sum_{i=1}^{n}\left(\frac{c_{R_i}(\omega)A_{R_i}(\omega)}{\omega}\right)^2\left\{1+\left(\frac{\alpha^2}{2}\right)\left(\frac{u}{w}\right)_i^2(\omega)\right\} \tag{6}$$

$$P_{HL}(\omega) = \sum_{i=1}^{n}\left(\frac{\alpha^2}{2}\right)\left(\frac{c_{L_i}(\omega)A_{L_i}(\omega)}{\omega}\right)^2 \tag{7}$$

where, A_{Ri} and A_{Li} are ith mode of medium response of Rayleigh and Love waves respectively, c_{Ri} and c_{Li} are ith mode of phase velocity of Rayleigh and Love waves respectively. u/w_i is H/V ratio or ellipticity of Rayleigh mode at free surface. The A_{Ri}, A_{Li}, c_{Ri}, c_{Li}, and u/w_i can be calculated from a 1D velocity profile. The P_{HS} and P_{VS} are the horizontal and vertical power of surface waves respectively. The P_{HR} and P_{VR} are the horizontal and vertical power of Rayleigh waves and P_{HL} is the horizontal power of Love waves. α is the H/V ratio of loading force.

The inversion was performed based on minimization of differences between the observed and the effective mode phase velocities and HVSR (Suzuki and Yamanaka, 2010). An objective function in the inversion can be written as

$$E = \varepsilon_{PV}E_{PV} + \varepsilon_{HV}E_{HV} + \varepsilon_{HVP}E_{HVP} \tag{8}$$

$$E_{PV} = \left(\frac{1}{N_{PV}}\right)\sum_{i=1}^{N_{PV}}\left[\frac{c_O(\omega_i) - c_e(\omega_i)}{c_O(\omega_i)}\right]^2 \tag{9}$$

$$E_{HV} = \left(\frac{1}{N_{HV}}\right)\sum_{i=1}^{N_{HV}}\left[\frac{H/V_O(\omega_i) - H/V_{Se}(\omega_i)}{H/V_O(\omega_i)}\right]^2 \tag{10}$$

$$E_{HVP} = \left[\frac{T_O - T_C}{T_O}\right]^2 \tag{11}$$

$$\varepsilon_{PV} + \varepsilon_{HV} + \varepsilon_{HVP} = 1 \tag{12}$$

where E is the error to be minimized in the inversion, E_{PV}, E_{HV} and E_{HVP} are the errors associated with the phase velocities, HVSR, and the peak frequency of the HVSR respectively. The $c_O(\omega)$ and $c_e(\omega)$ are the observed and theoretical (effective mode) phase velocities, $H/V_O(\omega)$ and $H/V_{Se}(\omega)$ are the observed and theoretical (effective mode) HVSR, T_O and T_C are the observed and theoretical peak frequency of the HVSR. The N_{PV} and N_{HV} are the number of phase velocity and HVSR data respectively. The ε_{PV}, ε_{HV}, and ε_{HPV} are the weight coefficients for the phase velocities, HVSR, and the peak frequency of the HVSR respectively. The weight is the largest for the phase velocities and the smallest for the peak frequency of the HVSR in this investigation.

An example of observed and theoretical dispersion curves at Pleasanton (site 59) is shown in Fig. 4, the observed curve is shown in red and the yellow circles indicate the effective mode of theoretical phase velocities. The theoretical dispersion curve (effective mode) agrees reasonably well with the observed data. An example of observed and theoretical HVSR from Site 84 (Eden Shores Park) is shown in Fig. 5. The theoretical (effective mode) HVSR (filled yellow circles) is generally consistent with the observed data (magenta line with small black dots), including a peak at a frequency of 0.5 Hz.

4. Investigation results

4.1. Dispersion curves

Fig. 6 shows a comparison of dispersion curves for five sites from Pleasanton to Alameda. Phase velocities for frequencies below 5 Hz at Site 58 (Castro Valley), located between the Hayward and Calaveras faults, are clearly higher than those at other locations. Site 69 (Pleasanton), which lies within a few hundred meters of the Calaveras fault, has phase velocities that are higher than three other sites that are located further away from the East Bay Hills block and presumably underlain by thicker sediments. At Site 59 (Pleasanton) and Site 57 (Alameda), the longest

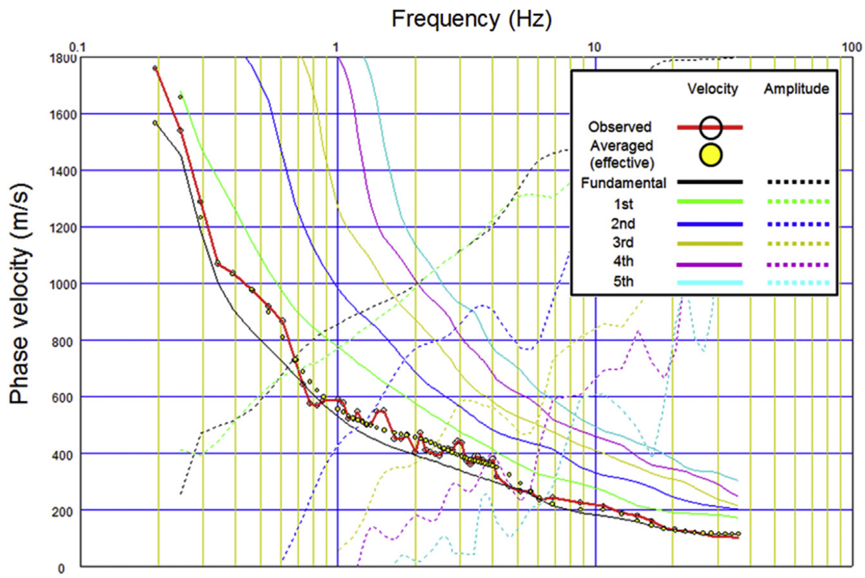

Fig. 4. Comparison of observed and theoretical dispersion curves (Site 59: Pleasanton). Red solid line with white circles indicates observed dispersion curve. Solid and broken lines indicate fundamental and higher modes theoretical dispersion curves and their relative amplitude (response of the medium). Yellow circles indicate the effective mode of theoretical phase velocities. (For interpretation of the references to colour in this figure legend, the reader is referred to the web version of this article.)

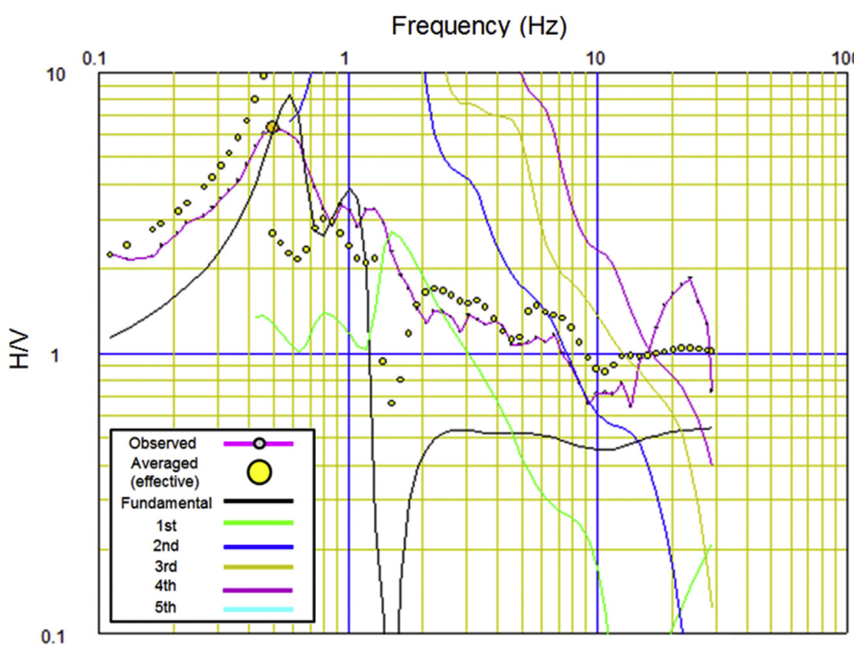

Fig. 5. Comparison of observed and theoretical horizontal to vertical spectral ratio (HVSR) (Site 84: Eden Shores Park). Magenta solid line with black dots indicates observed HVSR. Solid lines indicate fundamental and higher modes theoretical HVSR. Yellow circles indicate the effective mode of theoretical HVSR. (For interpretation of the references to colour in this figure legend, the reader is referred to the web version of this article.)

wavelengths associated with observed phase velocities are greater than 5 km and may include information on the S-wave velocity structure to a depth of 2000–3000 m. The maximum Rayleigh-wave phase velocities at these sites are about 1700 m/s, which implies that S-wave velocity at depths of 2000–3000 m is greater than 1700 m/s.

Dispersion curves for six sites in Hayward may be compared in Fig. 7. Phase velocities at the Site 64 (CSU East Bay), located immediately to the east of the Hayward fault, are substantially higher than those at the other four sites. Phase velocities decrease from east to west, for example, from Site 68 (Cemetery) to Site 84 (Eden Shores Park), as the distance from the Hayward fault increases. Horizontal to vertical spectral ratio (HVSR) for six sites in Hayward is shown in Fig. 8. There is no clear peak in a HVSR at Site 64 (CSU East Bay), located immediately to the east of the Hayward fault. In contrast, there are clear peaks in the HVSR of Sites 68 (Cemetery) to 84 (Eden Shores Park). The peaks decrease from 1.5 Hz to 0.5 Hz as distance from the Hayward fault increases. Both changes of dispersion curves and HVSRs indicate that S-wave velocity decreases from east to west as distance from the Hayward Faults increases and the basin sediments evidently thicken.

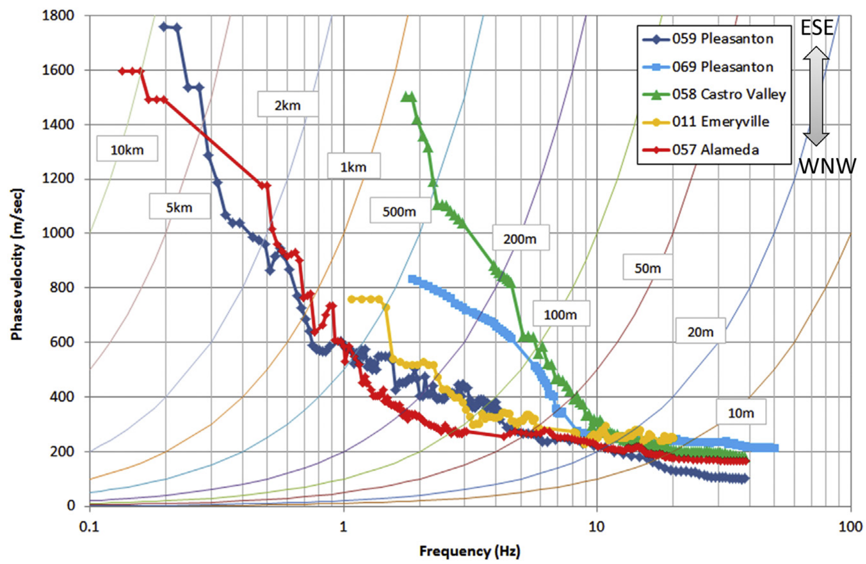

Fig. 6. Comparison of dispersion curves (Pleasanton to Alameda).

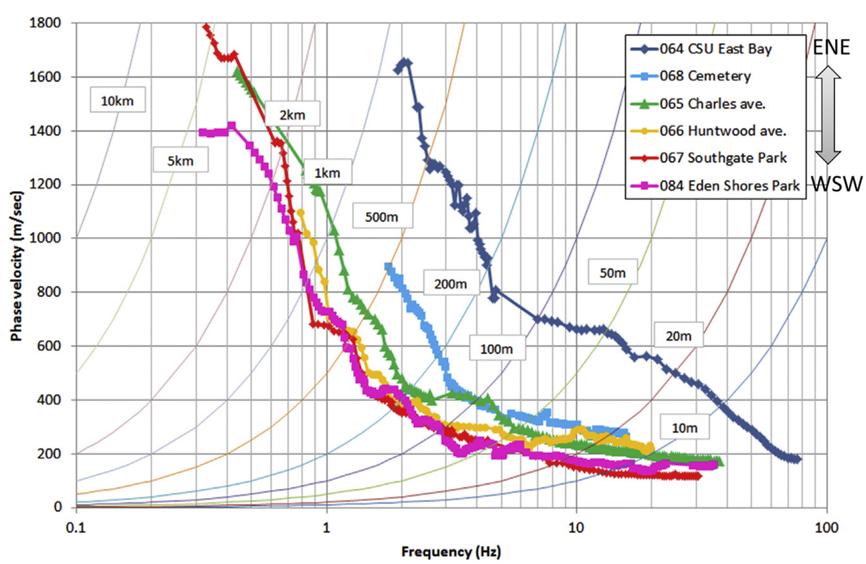

Fig. 7. Comparison of dispersion curves (Hayward).

4.2. S-wave velocity profiles

A comparison of S-wave velocity profiles from Pleasanton to Alameda is shown in Fig. 9. At Sites 59 (Pleasanton) and 57 (Alameda), S-wave velocity profiles were determined to a depth greater than 1500 m. S-wave velocity profiles were determined to a depth of several hundred meters at three other sites (69, 58 and 11). The penetration depth at these sites was limited because the maximum sensor separation was smaller than at other sites. At all five of these sites, there is a near-surface layer with S-wave velocity less than 300 m/s. A shallow stiff sediment layer with S-wave velocity more than 300 m/s was determined at a depth ranging from 15 to 50 m, depending on the site. This layer was relatively deep at Site 57 (Alameda). An intermediate velocity layer with S-wave velocity greater than 700 m/s was calculated for a depth range from 30 to 300 m. This layer was shallow at Sites 69 (Pleasanton) and 58 (Castro Valley). A layer with S-wave velocity greater than 1500 m/s was measured at Sites 59, 58 and 57. Depth to the layer is about 200 m at Site 58 (Castro Valley) and about 1700 m at Sites 59 (Pleasanton) and 57 (Alameda).

A comparison of S-wave velocity profiles at Hayward is shown in Fig. 10. At Sites 67 (Southgate Park) and 84 (Eden Shores Park), S-wave velocity profiles were determined to a depth greater than 1500 m. S-wave velocity profiles were determined to a depth of approximately 400 m at Site 64 (CSU East Bay), 800 m at Sites 68 (Cemetery) and 66 (Huntwood), and 1200 m at Site 65 (Charles Ave.). The relatively shallow penetration depth at these four sites compared with Sites 67 and 84 was because of a limited maximum sensor separation. A very thin near-surface layer (about 4 m thick) with S-wave velocity less than 300 m/s is present at Site 64 (CSU East Bay). At five other sites, a shallow stiff sediment layer with S-wave velocity more than 300 m/s was determined at a depth ranging from 8 to 53 m, depending on the site. An intermediate velocity layer with S-wave velocity greater than 700 m/s was calculated for a depth range from 40 to 250 m. This layer was shallow at Site 64 (CSU East Bay) and progressively deeper from

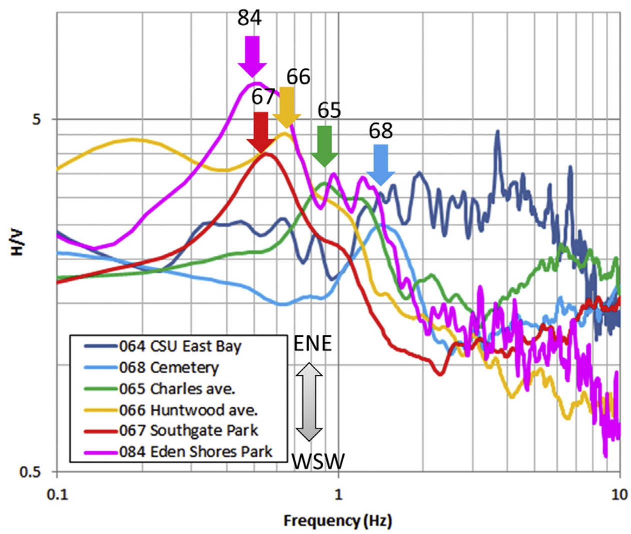

Fig. 8. Comparison of horizontal to vertical spectral ratio (HVSR) at Hayward.

east (Site 68) to west (Site 84), as distance from the Hayward Fault to each site increases. A velocity layer with S-wave velocity greater than 1200 m/s was detected at all sites. The depth to the layer is about 160 m at Site 64 and 400–700 m at other sites. A velocity layer with S-wave velocity greater than 1500 m/s was determined at a depth of about 200 m at Site 64 (CSU East Bay), 800 m at Site 65 (Charles Ave.), and greater than 1400 m at Sites 67 (Southgate Park) and 84 (Eden Shores Park).

A schematic S-wave velocity section based on the S-wave velocity profiles obtained by this study is shown in Fig. 11. The horizontal axis indicates distance from the Hayward fault to each investigation site. S-wave velocity profiles show significant differences among the sites. On the west side of the Hayward fault and the east side of the Calaveras fault, there is a low velocity layer at the surface, with S-wave velocity less than 700 m/s to a depth of 100–300 m. A thick intermediate velocity layer with S-wave velocity ranging from 700 to 1500 m/s lies beneath the low velocity layer. Bedrock with S-wave velocity greater than 1500 m/s was measured at a depth of approximately 1700 m. Between the Hayward fault and the Calaveras fault, thicknesses of the low velocity layer and the intermediate velocity layer are less than 50 m and 250 m respectively. Depth to bedrock is less than 300 m at these sites.

As we cross the Hayward fault from east to west, depths to an intermediate velocity layer with S-wave velocity greater than 700 m/s and a layer with S-wave velocity greater than 1200 m/s increase about 40 and 300 m respectively between Site 64 and Site 68, which are only 800 m apart. Depth to a bedrock with S-wave velocity greater than 1500 m/s increases by at least 500 m as well. These results are consistent with a seismic reflection survey of Williams et al. (2005) that shows a vertical offset of bedrock depth of approximately 400 m across the Hayward fault in Fremont.

5. Two dimensional amplification across the Hayward fault

To evaluate the effect of a significant lateral change of bedrock depth on surface ground motion due to an earthquake, a representative S-wave velocity cross section perpendicular to the Hayward fault was constructed and theoretical amplification of S_H waves including two-dimensional (2D) structure was calculated using a viscoelastic finite-difference method.

The representative S-wave velocity cross section based on the results of the present study is shown in Fig. 12a. A two-dimensional viscoelastic velocity-stress staggered grid finite-difference method (Levander, 1988; Robertsson et al., 1994) was used for calculating 2D amplification. Topographic relief was taken into account in the calculation (Hayashi et al., 2001). Grid size is 5 m, density is constant, and Q is 100 throughout a model. A plane S_H wave was initiated at the bottom of the model and response at the ground surface was recorded. The surface ground motion was divided by the initiated wave and examined in frequency domain as amplification. To evaluate the effect of 2D structure, 1D amplification was also calculated by a reflectivity method (Thomson, 1950; Mueller, 1985).

Horizontal ground motion at the surface including 2D structure calculated by the finite-difference method is shown in Fig. 12b. There is a clear direct arrival around 2 s. We can see another clear wave packet propagating left (west) from a distance of 3500 m. Phase velocities of the wave packets are in the range of Love waves, implying that the incident plane S_H wave is converted to Love waves at the horizontal velocity change associated with the Hayward fault.

The 1D and 2D amplifications of SH waves are shown in Fig. 12c. The vertical axis is frequency and the color indicates the

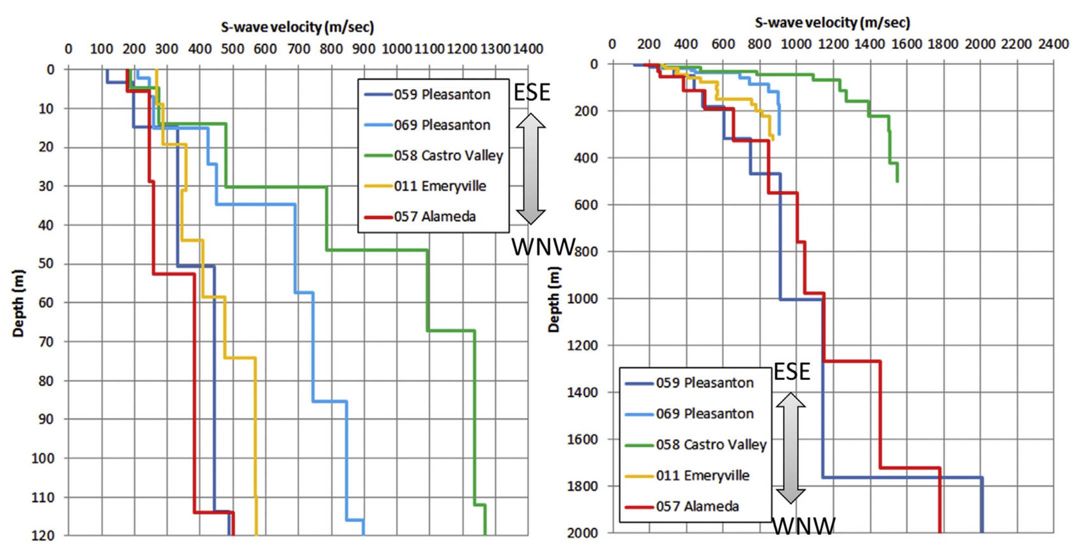

Fig. 9. Comparison of S-wave velocity profiles from Pleasanton to Alameda.

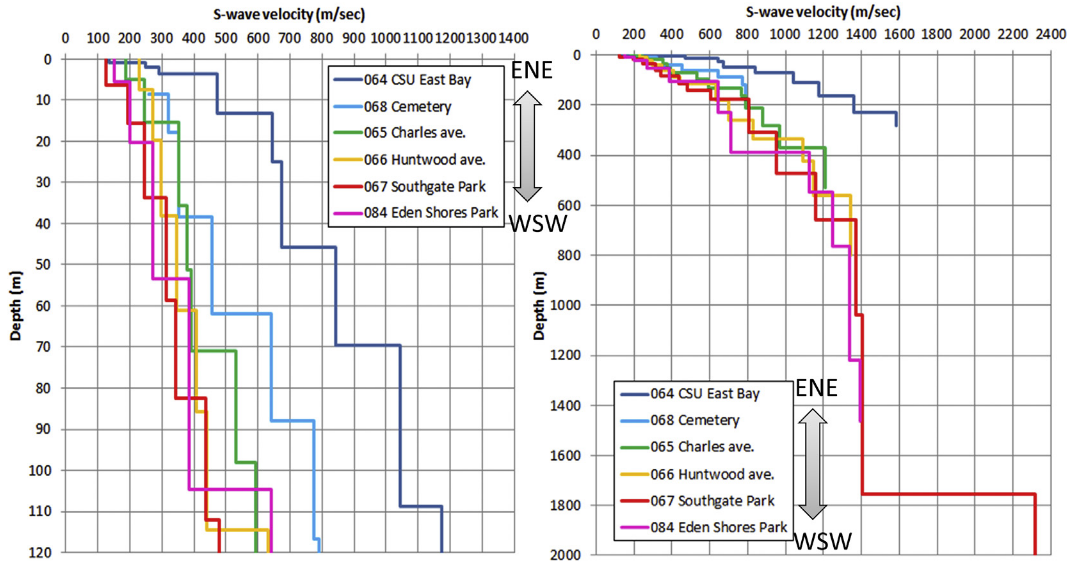

Fig. 10. Comparison of S-wave velocity profiles at Hayward.

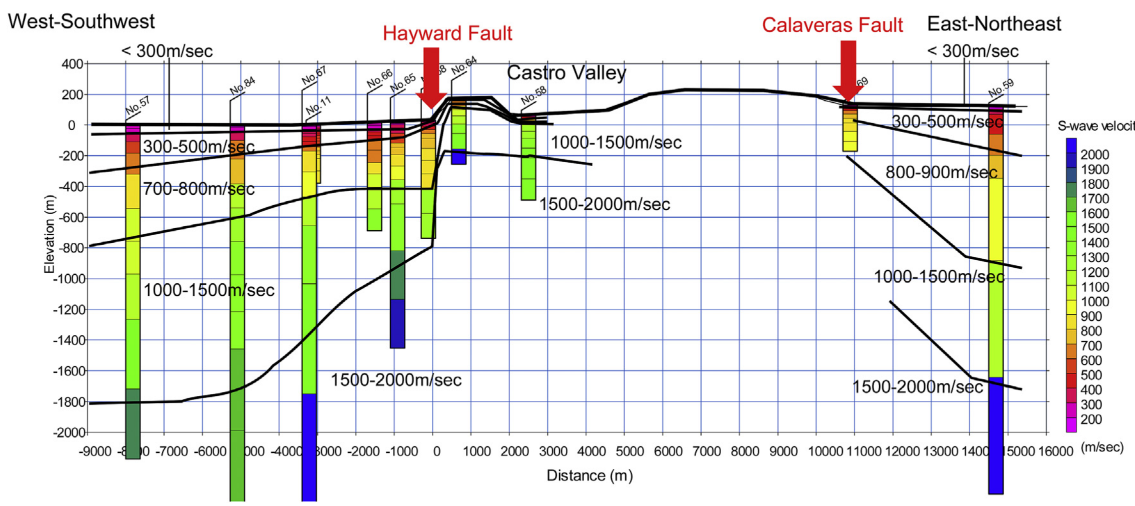

Fig. 11. Schematic S-wave velocity section based on the S-wave velocity profiles obtained in this study.

amplification. Blue to green colors indicate small amplitudes and yellow to red colors indicate large amplitudes. On the left hand (west) side of the Hayward fault, amplitude is large at frequencies of about 1 Hz and 4 Hz. Amplification is clearly larger in the 2D calculation than in the 1D calculation.

A comparison of maximum amplification in the frequency range of 0–5 Hz is shown in Fig. 13. On the west side of the Hayward fault, 2D amplification at a frequency of 1 Hz is approximately 6 times that of incident waves. The 2D amplification is particularly large (7–8 times) at distances of 700 and 2500 m (2800 and 1000 m from the Hayward Fault respectively). In contrast, amplification is only about 4 times in the 1D calculation. The calculation results imply that the low frequency (0.5–5 Hz) component of ground motion can be locally amplified on the west side of the Hayward fault because of the effect of a lateral change of in the depth of basement.

6. Discussion of uncertainties in phase velocity determination and inversion

Velocity models determined using of surface wave methods are non-unique, it is very difficult to obtain unique and reliable solutions without uncertainty from waveform data obtained on the ground surface. The section discusses the uncertainties associated with phase velocity determination using linear arrays and inversion from a site amplification point of view.

6.1. Phase velocity determination using linear arrays

Isotropic array patterns such as a circle or equilateral triangle provide more consistent velocity measurements than anisotropic arrays such as a linear array in the presence of anisotropic ambient noise. The anisotropic arrays, however, do provide reliable phase velocity information when ambient noise propagates in many directions. Hayashi and Kita (2010) demonstrated that a linear array can provide usable phase velocities when propagation direction of ambient noise is distributed over a range of at least 120°. In order to evaluate the applicability of the anisotropic array, we need to consider the azimuthal distribution the propagation direction of ambient noise. To investigate the azimuthal variation in propagation directions, ambient noise was analyzed using sensor pairs with

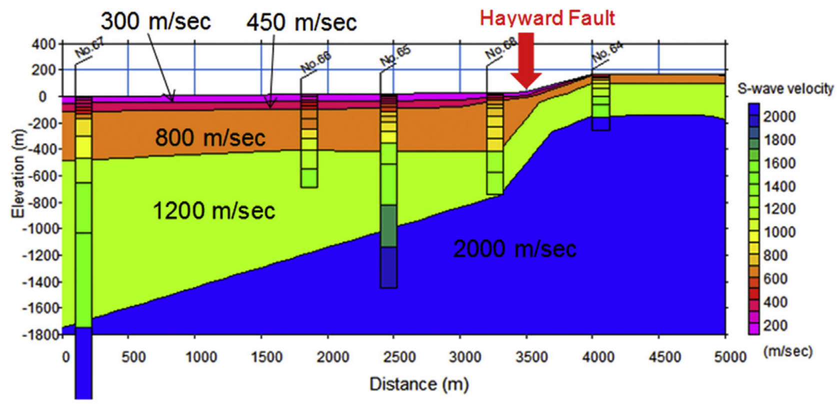

a) Representative S-wave velocity cross section perpendicular to the Hayward Fault.

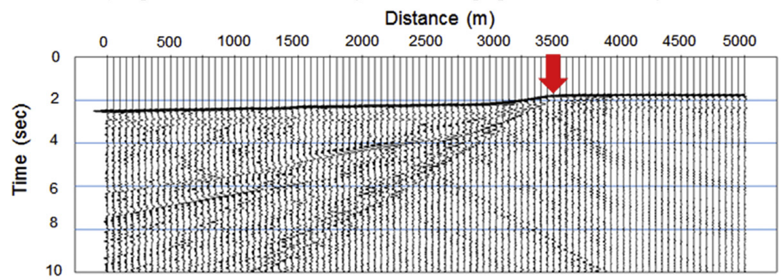

b) Horizontal ground motion at the surface.

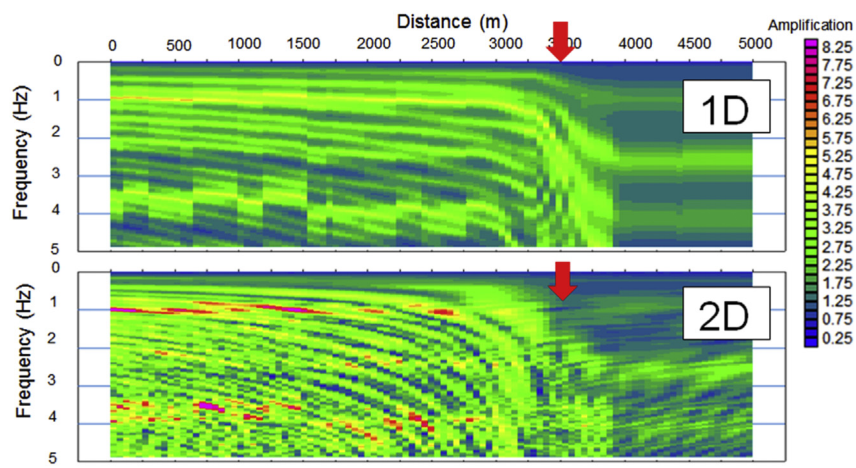

c) 1D amplification of SH waves calculated by a reflectivity method without 2D effect (top) and 2D amplification of SH waves calculated by a finite-difference method including 2D effect (bottom).

Fig. 12. 2D Amplification across the Hayward fault.

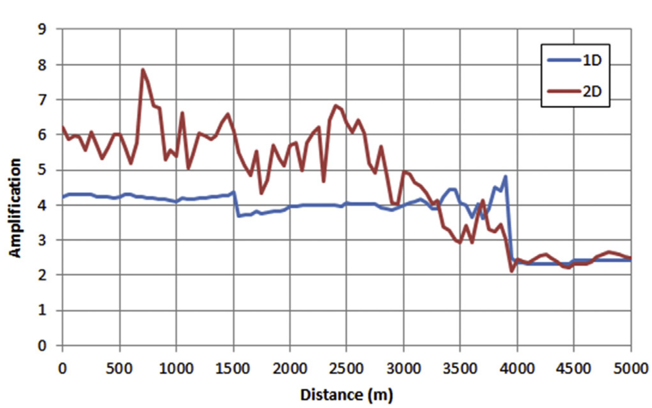

Fig. 13. Comparison of maximum amplification in a frequency range of 0–5 Hz.

several different orientations. Fig. 14 shows an example of coherencies calculated from two-sensor linear arrays with different orientations. Fig. 14a and b show small and large arrays for high and low frequency observations, respectively. Fig. 14c and d are coherencies calculated from sensor pairs shown in Fig. 14a and b, respectively. We can see that coherencies are almost identical in the frequency ranges of interest, 1.5–5 Hz for the small array (Fig. 14c) and 0.2–0.5 Hz for the large array (Fig. 14d), regardless the direction of sensor pairs. This implies that the ambient noise is generally omnidirectional in the investigation area. This may be explained by the tendency for surface waves to be scattered by lateral heterogeneities in the near surface zone as well as topographic features. The urban environment contains a plethora of sources that generate surface waves including motor vehicles, machinery, etc. By the time the wavefields from multiple sources have been multiply scattered, the resultant ambient noise field is remarkably

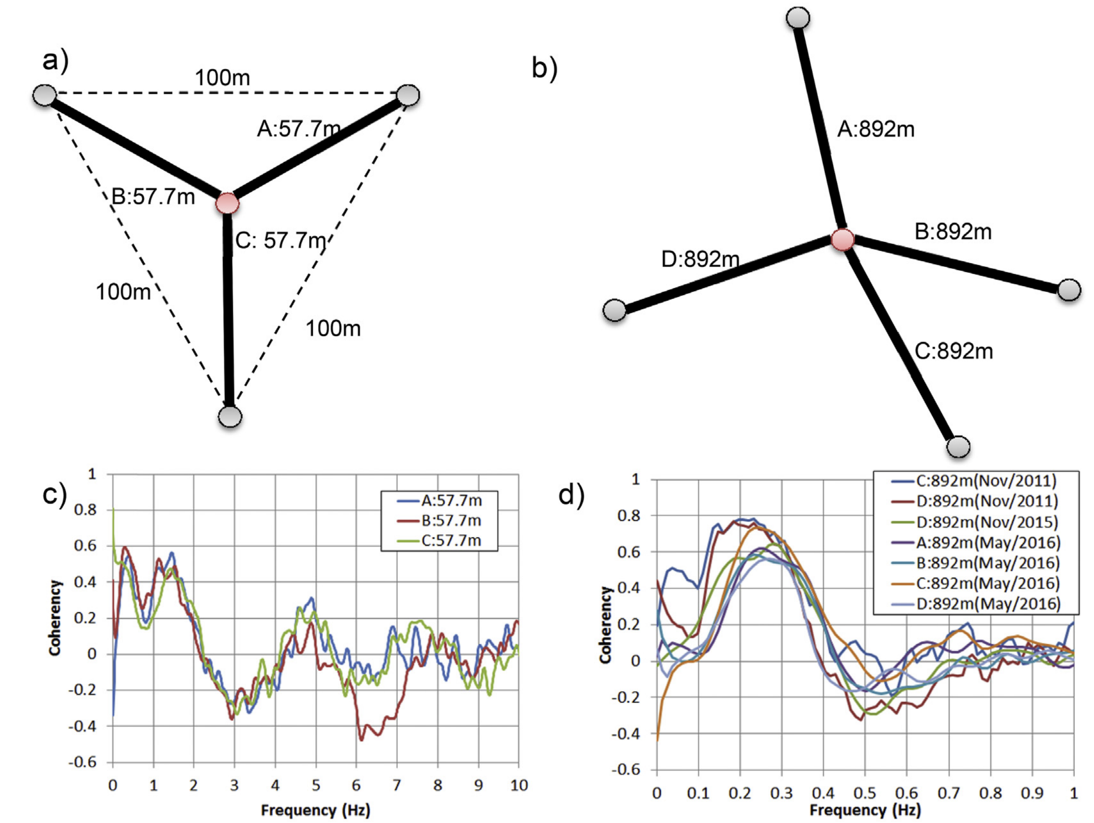

Fig. 14. Example of coherencies calculated from linear arrays with different directions. a) Array configuration for high frequency measurements. b) Array configuration for low frequency measurements. c) Coherencies calculated from a small array (a). d) Coherencies calculated from a large array (b).

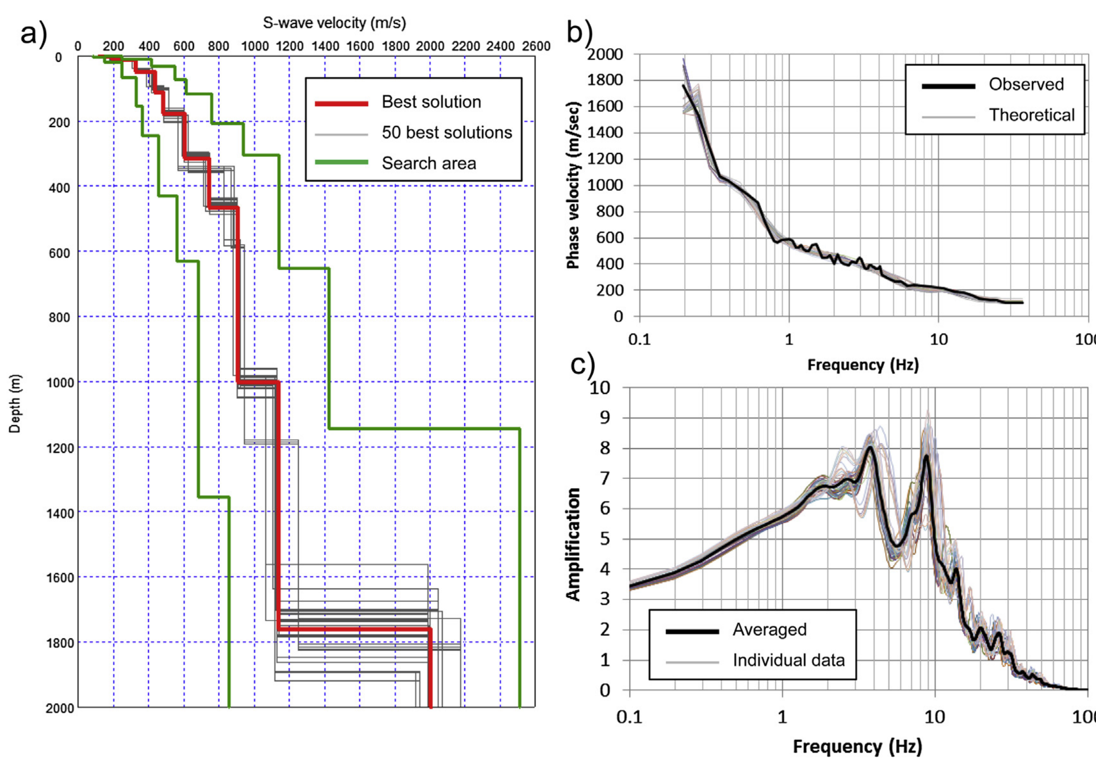

Fig. 15. Example of uncertainty analysis. a) Best (bold red line) and other 50 best (thin gray lines) solutions with a search area (bold green line) of the genetic algorithm. b) Theoretical phase velocities (thin gray lines) in comparison with observed data (bold black line). c) Theoretical 1D amplification (thin gray lines) calculated from the 50 best models shown in (a) with average amplification (bold black line) of the 50 models. (For interpretation of the references to colour in this figure legend, the reader is referred to the web version of this article.)

omnidirectional. The uncertainty associated with anisotropic arrays can be evaluated by comparing coherencies with ones obtained by multi-directional arrays.

6.2. Inversion and site amplification uncertainty

Several different velocity profiles that yield almost the same theoretical phase velocities were examined to evaluate the effect of uncertainty of inversion on amplification calculation. Fig. 15 shows an example of uncertainty analysis. An inversion using a genetic algorithm was performed seven times and the 50 best solutions were compared. Fig. 15a shows the 50 best solutions with the search area of the genetic algorithm. Fig. 15b shows theoretical phase velocities in comparison with observed data. The theoretical phase velocities of the 50 best solutions are almost identical and it is difficult to select the best profile. This is a typical example of non-uniqueness in the inversion of geophysical data. The amount of variation in the velocity model in Fig. 15a indicates the magnitude of uncertainty, dependent on depth. The uncertainty is relatively large at the depths of 400 m, 1000–1200 m, and 1500–1900 m. The number of layers was fixed at 10 throughout the analysis, and the uncertainty could be larger if the number of layers was variable. Fig. 15c shows theoretical 1D amplification calculated from the 50 best solutions shown in Fig. 15a. We can see that the peaks of amplifications, 4 Hz and 9 Hz are consistent throughout the 50 solutions regardless the uncertainty of velocity profiles. The inversion of the dispersion curve is non-unique and the uncertainty is generally increasing with depth since the sensitivity or resolution of phase velocity is decreasing with depth. The sensitivity or resolution of surface site amplification, however, is also decreasing with depth so that the effect of uncertainty associated with surface wave inversion on the surface site amplification is not significant. The results shown here demonstrate the general applicability of surface wave methods to the evaluation of site amplification regardless the uncertainty of the surface wave inversion.

7. Conclusions

S-wave velocity profiles were determined at eleven sites in the east San Francisco Bay area using surface geophysical methods. Resultant S-wave velocity profiles show significant differences among the sites. Across the Hayward fault, depth to bedrock with S-wave velocity greater than 1500 m/s changes at least 500 m. To evaluate the effect of a significant lateral change of bedrock depth on surface ground motion due to earthquakes, an S-wave velocity cross section perpendicular to the Hayward fault was constructed and theoretical amplification including the effect of two-dimensional structure was calculated using a viscoelastic finite-difference method. Calculation results show that the low frequency component of ground motion is locally amplified on the west side of the Hayward Fault because of the effect of two-dimensional structure.

The results of this investigation indicate that the phase velocity information obtained using the 2ST-SPAC method with a limited number of high quality sensors provides valuable S-wave velocity information over a wide depth range. It offers a robust alternative to widely-used single station methods such as the horizontal to vertical spectral ratio. Though the 2ST-SPAC method and other passive surface wave methods using an anisotropic or linear array cannot equal the performance of an isotropic array in the case of strongly anisotropic ambient noise, they do provide an effective alternative for many urban environments where ambient noise is relatively isotropic and potential sites for array deployment are limited to corridors along roadways.

Although the inversion of surface wave data is essentially non-unique and we cannot remove uncertainty from analyses, the effect of the uncertainty depends on the purpose of investigation and the use of the data. Site amplifications calculated from S-wave velocity profiles are relatively insensitive to uncertainties in the velocity profiles.

Acknowledgements

The authors thank Larry Lepore of the Hayward Area Recreation and Park District for providing access to sites in Hayward and Castro Valley. Mark Spiller of the City of Pleasanton helped to arrange access to the Pleasanton Sports Park. Seth Shuler and Rania Aql of California State University, East Bay, assisted with data acquisition. Two anonymous reviewers provided constructive comments that improved the quality of the paper.

References

Aki, K., 1957. Space and time spectra of stationary stochastic waves, with special reference to microtremors. Bull. Earthq. Res. Ins. 35, 415–456.
Arai, H., Tokimatsu, K., 2000. Effects of Rayleigh and Love waves on microtremor H/V spectra. In: Proceedings of 12th World Conference on Earthquake Engineering article 2232.
Asten, M.W., 2006. On bias and noise in passive seismic data from finite circular array data processed using SPAC methods. Geophysics 71, V153–V162.
Craig, M.S., Genter, R.L., 2006. Geophone array formation and semblance evaluation. Geophysics 71, Q1–Q8.
Field, E.H., Biasi, G.P., Bird, P., Dawson, T.E., Felzer, K.R., Jackson, D.D., Johnson, K.M., Jordan, T.H., Madden, C., Michael, A.J., Milner, K.R., Page, M.T., Parsons, T., Powers, P.M., Shaw, B.E., Thatcher, W.R., Weldon, R.J., Zeng, Y., 2015. Long-term time-dependent probabilities for the third uniform California earthquake rupture forecast (UCERF3). Bull. Seismol. Soc. Am. 111, 511–543.
Garofalo, F., Foti, S., Hollender, F., Bard, P.Y., Cornou, C., Cox, B.R., Ohrnberger, M., Sicilia, D., Asten, M., Di Giulio, G., Forbriger, T., Guillier, B., Hayashi, K., Martin, A., Matsushima, S., Mercerat, D., Poggi, V., Yamanaka, H., 2016a. InterPACIFIC project: comparison of invasive and non-invasive methods for seismic site characterization. Part I: intra-comparison of surface wave methods. Soil Dyn. Earthq. Eng. 82, 222–240.
Garofalo, F., Foti, S., Hollender, F., Bard, P.Y., Cornou, C., Cox, B.R., Dechamp, A., Ohrnberger, M., Perron, V., Sicilia, D., Teague, D., Vergniault, C., 2016b. InterPACIFIC project: comparison of invasive and non-invasive methods for seismic site characterization. Part II: inter-comparison between surface-wave and borehole methods. Soil Dyn. Earthq. Eng. 82, 241–254.
Hayashi, K., Burns, D.R., Toksöz, M.N., 2001. Discontinuous grid finite-difference seismic modeling including surface topography. Bull. Seismol. Soc. Am. 91, 1750–1764.
Hayashi, K., Hirade, T., Iiba, M., Inazaki, T., Takahashi, H., 2008. Site investigation by surface-wave method and micro-tremor array measurements at central Anamizu, Ishikawa Prefecture. BUTSURI-TANSA 61, 483–498 (in Japanese).
Hayashi, K., 2009. Effect of array shape on the spatial auto-correlation analysis of micro-tremor array measurements. In: Proceedings of the Symposium on the Application of Geophysics to Engineering and Environmental Problems 2009, pp. 616–625.
Hayashi, K., Kita, T., 2010. Applicability of a spatial autocorrelation method (SPAC) using a linear array in comparison with triangle and L-shaped arrays. In: Proceedings of the Symposium on the Application of Geophysics to Engineering and Environmental Problems 2010.
Hayashi, K., Underwood, D., 2012a. Estimating deep S-wave velocity structure using microtremor array measurements and three-component microtremor array measurements in San Francisco Bay area. In: Proceedings of the Symposium on the Application of Geophysics to Engineering and Environmental Problems 2012.
Hayashi, K., Underwood, D., 2012b. Microtremor array measurements and three-component microtremor measurements in San Francisco Bay area. In: 15th World Conference on Earthquake Engineering 2012, p. 1634.
Hayashi, K., Cakir, R., Dragovich, J. D, Stoker, B. A, Walsh, T. J., and Littke, H., 2013a, A passive Seismic Analyses in the Sultan 7.5-minute quadrangle, King and Snohomish Counties, Washington: Washington Division of Geology and Earth Resources Open File Report 2013-01, 9.
Hayashi, K., Martin, A., Hatayama, K., Kobayashi, T., 2013b. Estimating deep S-wave velocity structure in the Los Angeles Basin using a passive surface wave method. Lead. Edge 32, 620–626.
Ikeda, T., Matsuoka, T., Tsuji, T., Hayashi, K., 2012. Multimode inversion with amplitude response of surface waves in the spatial autocorrelation method. Geophys. J. Int. 190, 541–552.
Kawase, H., 1996. Cause of the damage belt in Kobe: "The Basin-Edge effect," constructive interference of the direct S-Wave with the basin-induced diffracted/Rayleigh waves. Seismol. Res. Let. 67-5, 25–34.
Levander, A.R., 1988. Fourth-order finite-difference P-SV seismograms. Geophysics

53, 1425–1436.

Louie, J.M., 2001. Faster, better: shear-wave velocity to 100 meters depth from refraction microtremor arrays. Bull. Seismol. Soc. Am. 91, 347–364.

Margaryan, S., Yokoi, T., Hayashi, K., 2009. Experiments on the stability of the spatial autocorrelation method (SPAC) and linear array methods and on the imaginary part of the SPAC coefficients as an indicator of data quality. Explor. Geophys. 40, 121–131.

Miller, R.D., Xia, J., Park, C.B., Ivanov, J.M., 1999. Multichannel analysis of surface waves to map bedrock. Lead. Edge 18, 1392–1396.

Mueller, G., 1985. The reflectivity method: a tutorial. J. Geophys. 58, 153–174.

Mykkeltveit, S., Astebol, K., Doornbos, D.J., Husebye, E.S., 1983. Seismic array configuration optimization. Bull. Seismol. Soc. Am. 73, 173–186.

Nazarian, S., Stokoe, K.H., Hudson, W.R., 1983. Use of spectral analysis of surface waves method for determination of moduli and thickness of pavement system. Transp. Res. Rec. 930, 38–45.

Obuchi, T., Yamamoto, H., Sano, T., Saito, T., 2004. Estimation of underground velocity structure based on both fundamental and highermodes. In: Proceedings of the 111th SEGJ Conference, Society of Exploration Geophysicists of Japan, pp. 25–28 (in Japanese with English abstract).

Okada, H., 2003. The Microtremor Survey Method. Society of Exploration Geophysicist, Tulsa.

Park, C.B., Miller, R.D., Xia, J., 1999a. Multimodal analysis of high frequency surface waves. Proc. Symp. Appl. Geophys. Eng. Environ. Probl. 99, 115–121.

Park, C.B., Miller, R.D., Xia, J., 1999b. Multichannel analysis of surface waves. Geophysics 64, 800–808.

Robertsson, J.O.A., Blanch, J.O., Symes, W.W., 1994. Viscoelastic finite-difference modeling. Geophysics 59, 1444–1456.

Stephenson, W.J., Louie, J.N., Pullammanappallil, S., Williams, R.A., Odum, J.K., 2005. Blind shear-wave velocity comparison of ReMi and MASW results with boreholes to 200 m in santa clara valley: implications for earthquake ground-motion assessment. Bull. Seismol. Soc. Am. 95, 2506–2516. http://dx.doi.org/10.1785/0120040240.

Suzuki, H., Yamanaka, H., 2010. Joint inversion using earthquake ground motion records and microtremor survey data to S-wave profile of deep sedimentary layers. BUTSURI-TANSA 2010 65, 215–227 (in Japanese).

Tokimatsu, K., Arai, H., Asaka, Y., 1996. Deep shear-wave structure and earthquake ground motion characteristics in Sumiyoshi area, Kobe city, based on microtremor measurements. J. Struct. Constr. Eng. 491, 37–45.

Tokimatsu, K., 1997. Geotechnical site-characterization using surface-waves. In: Ishihara (Ed.), Earthquake geotechnical engineering. Balkema, Rotterdam, pp. 1333–1368.

Thomson, W.T., 1950. Transmission of elastic waves through a stratified solid medium. J. Appl. Phys. 2.1, 89.

Vermeer, G.J.O., 2002. 3-D Seismic Survey Design: SEG.

Wapenaar, K., 2004. Retrieving the elastodynamic Green's function of an arbitrary inhomogeneous medium by cross correlation. Phys. Rev. Lett. 93. Article 254301.

Williams, R.A., Simpson, R.A., Jachens, R.C., Stephenson, W.J., Odum, J.K., Ponce, D.A., 2005. Seismic reflection evidence for a northeast-dipping Hayward fault near Fremont, California: implication for seismic hazard. Geophys. Res. Lett. 32, L13301.

Xia, J., Miller, R.D., Park, C.B., 1999a. Configuration of near surface shear wave velocity by inverting surface wave. Proc. Symp. Appl. Geophys. Eng. Environ. Probl. 1999, 95–104.

Xia, j., Miller, R.D., Park, C.B., 1999b. Estimation of near-surface shear-wave velocity by inversion of Rayleigh waves. Geophysics 64, 691–700.

Yamanaka, H., Ishida, J., 1995. Phase velocity inversion using genetic algorithms. J. Struct. Constr. Eng. 468, 9–17 (in Japanese).

Yokoi, T., Hayashi, K., Aoike, K., 2006. A case study on dependence of the complex coherence function on the azimuth SPAC method of microtremor array measurement. In: Proceedings of the 114th SEGJ Conference, pp. 138–141 (in Japanese).